The Astrophysical Journal Letters, 987:L23 (9pp), 2025 July 1 https://doi.org/10.3847/2041-8213/ade670

Predictions for New Horizons' SWAP Measurements Downstream of the Heliospheric Termination Shock

E. J. Zirnstein[1], D. J. McComas[1], B. L. Shrestha[1], H. A. Elliott[2], P. C. Brandt[3], S. A. Stern[4], A. R. Poppe[5], J. Parker[4], E. Provornikova[3], K. Singer[4], A. Verbiscer[6], and
New Horizons Heliophysics Team
[1] Department of Astrophysical Sciences, Princeton University, Princeton, NJ 08544, USA; ejz@princeton.edu
[2] Southwest Research Institute, San Antonio, TX 78228, USA
[3] Johns Hopkins University Applied Physics Laboratory, Laurel, MD 20723, USA
[4] Southwest Research Institute, Boulder, CO 80302, USA
[5] Space Sciences Laboratory, University of California at Berkeley, Berkeley, CA 94720, USA
[6] Department of Astronomy, University of Virginia, Charlottesville, VA 22904, USA
Received 2025 May 15; revised 2025 June 20; accepted 2025 June 20; published 2025 July 1

Abstract

Currently ∼62 au from the Sun, the New Horizons spacecraft is en route to the outer heliosphere boundaries. The first boundary it will encounter is the heliospheric termination shock (HTS), where the solar wind ion (SWI) and interstellar pickup ion (PUI) plasma mixture is slowed down to subsonic speeds, compressed, and heated. Some particles, mostly PUIs, undergo preferential acceleration at the HTS due to their higher energies and thus gain the capability to reflect from the shock and undergo, e.g., shock drift acceleration. This produces a tail in the downstream PUI energy distribution, with the potential for multiple power-law breaks. In anticipation of crossing the HTS, we have constructed a test particle model with synthetic turbulence to simulate New Horizons' Solar Wind Around Pluto (SWAP) observations downstream of the HTS. SWAP can measure the energy/charge of multiple particle populations (thermal solar wind (SW) protons, alphas, and PUIs). Here, we calculate what SWAP might observe after it crosses the HTS. Our model shows that the count rate distribution will be very different from what is observed in the supersonic SW, with a hotter SW+PUI distribution and no sharp PUI cutoff. This will require a different method to quantify the moments of the SWIs and PUIs in the heliosheath. SWAP may be able to observe part of the PUI tail downstream of the HTS, if the upstream SW speed is $\lesssim$300 km s^{-1}. Moreover, if the shock compression ratio is also $\gtrsim$2, SWAP may observe multiple populations of the accelerated PUI distribution.

Unified Astronomy Thesaurus concepts: Heliosphere (711); Pickup ions (1239); Termination shock (1690); Solar wind (1534); Interplanetary particle acceleration (826)

1. Introduction

The New Horizons Solar Wind Around Pluto (SWAP) instrument (D. McComas et al. 2008) has been measuring interstellar H^+ PUIs from ∼11 au intermittently, and then nearly continuously from ∼22 to over 60 au from the Sun (H. A. Elliott et al. 2016; D. J. McComas et al. 2017, 2021, 2022, 2025; E. J. Zirnstein et al. 2022; B. L. Shrestha et al. 2025). SWAP is the only instrument that can measure and quantify the distribution of interstellar H^+ PUIs in the outer heliosphere. Interstellar H^+ PUIs are born, predominantly, by charge exchange with solar wind ions (SWIs) that are traveling supersonically away from the Sun (at speeds between ∼300 and 800 km s^{-1}). The newly ionized interstellar H^+ PUIs are then "picked up" (i.e., accelerated in the direction of the bulk solar wind (SW) plasma) by the motional electric field of the SW and become incorporated, but not thermalized, into the bulk SW plasma. The PUIs quickly form a shell velocity (or energy) distribution, whose speeds range from 0 to twice the SW speed in the solar inertial frame. Beyond ∼4 au (P. Swaczyna et al. 2020), the 1/e-folding interstellar neutral H ionization cavity (H. J. Fahr 1971; G. E. Thomas 1978), the majority of interstellar neutral H has already been ionized and picked up by the outward-propagating SW.

SWAP discovered that PUIs dominate the thermal plasma pressure beyond ∼20 au from the Sun (D. J. McComas et al. 2017, 2025). They are also preferentially accelerated at interplanetary shocks, forming downstream PUI tails (E. J. Zirnstein et al. 2018; B. L. Shrestha et al. 2024). By fitting power-law distributions to the PUI energy tails, SWAP observations have shown the PUI tails contain a significant amount of the pressure of the combined SW+PUI plasma (E. J. Zirnstein et al. 2018; B. L. Shrestha et al. 2024).

The heliospheric termination shock (HTS) is approximately stationary with respect the Sun and is one of the strongest shocks in the solar system. Numerous models have shown that the faster-moving PUIs should be preferentially accelerated at the HTS via their reflection from the shock and drift along the surface of the shock. This allows PUIs to gain energy from the upstream SW flow until they have high enough energies to cross downstream of the shock (R. H. Burrows et al. 2010; G. P. Zank et al. 2010; D. Ariad & M. Gedalin 2013; S. Matsukiyo & M. Scholer 2014; Z. Yang et al. 2015; J. Giacalone et al. 2021; E. J. Zirnstein et al. 2021). Lacking an instrument capable of observing interstellar H^+ PUIs, the Voyager spacecraft were unable to quantify their distributions in the outer heliosphere. Thus, for the first time SWAP will make these necessary revolutionary measurements when it crosses the HTS, and we will learn more about the shock properties and acceleration mechanisms responsible for the measured downstream PUI distributions.

In this study, we model the SWI+PUI distribution downstream of the HTS using a test particle simulation that uses a predefined mean shock profile superimposed by a synthetic turbulence spectrum to simulate the propagation and heating/acceleration of protons across the HTS. We aim to determine what SWAP might observe downstream of the HTS in the context of the instrument capabilities. We vary two different parameters of the simulation, i.e., the HTS compression ratio (2 and 2.5) and the upstream SW speed (300 and 400 km s^{-1}), and simulate each combination of these parameters (a total of four cases). We discuss the results in the context of SWAP's measurement capabilities, and what the accelerated PUI distribution looks like in SWAP's rest frame, thus offering a prediction of what SWAP might observe immediately downstream of the HTS.

2. Methodology

2.1. Test Particle Model

In our model, we simulate the propagation and acceleration of many test particles (∼3.8 million) and their interaction with the prescribed HTS structure, assumed to be stationary in the solar inertial frame, for each test case (see Figure 1). We follow E. J. Zirnstein et al. (2021) by solving for the transport of the particles across the HTS in the presence of a synthetic spectrum of turbulence, which we summarize in the Appendix. Particle trajectories are solved with the Lorentz force equation,

$$\frac{d\boldsymbol{v}_{\rm p}}{dt} = \frac{q}{m_{\rm p}}\left(\boldsymbol{E} + \frac{1}{c}\boldsymbol{v}_{\rm p} \times \boldsymbol{B}\right), \qquad (1)$$

where q is proton charge, $m_{\rm p}$ is proton mass, c is the speed of light, $\boldsymbol{v}_{\rm p}$ is the proton's velocity, the electric field $\boldsymbol{E} = -\frac{1}{c}\boldsymbol{u} \times \boldsymbol{B} - \nabla\Phi$, where $\boldsymbol{u}$ is the predetermined bulk plasma velocity $\boldsymbol{u} = u_x\hat{x}$ moving toward the shock, $\boldsymbol{B}$ is the total magnetic field, and Φ is the cross-shock potential (M. M. Leroy 1983; G. P. Zank et al. 1996; E. J. Zirnstein et al. 2021). Equation (1) is solved using the Bulirsch–Stoer method (W. H. Press et al. 2002) for every particle until it can be binned downstream of the shock.

We show the results of the downstream particle distributions as (1) speed distributions in the downstream plasma frame and (2) count rate distributions in a simulated spacecraft frame moving like New Horizons. To convert from the speed distribution in the spacecraft frame to count rates, we use the equation (D. J. McComas et al. 2021) $c_r = 1/2G^E v^4 f(v)$, where c_r is the count rate and G^E is the geometric factor of SWAP as a function of energy (B. M. Randol et al. 2012), which is accounted for in our simulation. Both SWIs (i.e., SW protons) and PUIs (i.e., pickup protons) are simulated with particle weights represented by a shell of the speed distribution, fv^2dv, depending on the randomized velocity a particle is given. The SWI distribution is represented by a Maxwell–Boltzmann distribution upstream of the shock with a temperature of 20,000 K, like what Voyager 2 observed upstream of the HTS (J. D. Richardson et al. 2008). A kappa distribution would be more appropriate based on SWAP observations (G. Livadiotis et al. 2024; D. J. McComas et al. 2025); however, we tested using the extrapolated kappa value of 4.3 and found little change in the results. The PUI distribution is represented by a generalized filled shell distribution upstream of the shock, with a relative PUI-to-total density of 30% and PUI cooling index of 2.9, values extrapolated from SWAP observations to 90 au from the Sun (D. J. McComas et al. 2021, 2025). They are extrapolated using power-law relationships fit to SWAP data. B. Wang et al. (2023) noted that the power-law relationship used to extrapolate the PUI cooling index from New Horizons' SWAP observations may not work due to the complexities of turbulence in the outer heliosphere, such as turbulence driven by PUIs or the heating of PUIs from a still unknown source. In fact, it has been shown that turbulence is spatially dependent and can behave differently in the outer heliosphere (G. P. Zank et al. 2018). In their theoretical model, B. Wang et al. (2023) also showed that a large PUI cooling index may cause a larger deviation between predicted and observed energetic neutral atom (ENA) flux at energies near ∼3 keV. While this should be kept in mind when interpreting our results, in the absence of good theoretical models of the radial trend of the PUI cooling index we adopt a power-law approach following D. J. McComas et al. (2021, 2025).

In this study, we assume the HTS is 90 au from the Sun, or less than 30 au beyond New Horizons' current position. We assume 90 au because it is approximately halfway between the HTS crossing distances of the two Voyager spacecraft. Some models might predict the HTS will be closer or farther away, but we expect this will make qualitatively little difference in the downstream SWI and PUI energy distributions (see the Appendix for more details).

3. Results

Figure 1 shows the mean field shock structure (black curves) for the four combinations of simulations chosen for this study. Using Equation (A3) in the Appendix of E. J. Zirnstein et al. (2021), we construct the mean field along the $+y$-axis that allows the creation of a PUI foot, ramp, and shock overshoot. Each case has the same PUI foot length (∼2 advective gyroradii in length), although with different amplitudes depending on the compression ratio. The length of the ramp to the overshoot is chosen to be 3 ion inertial lengths, but note they are different in units of $R_{\rm g}$ for $\boldsymbol{u}_{\rm up,sh} = 300$ versus 400 km s^{-1}. This is because the gyroradius scale is determined by a particle with speed $\boldsymbol{u}_{\rm up,sh}$ advecting with the same upstream plasma flow speed. The blue curves in Figure 1 are the kinetic energy of only the bulk plasma flow upstream through downstream of the shock, assuming $\boldsymbol{u} = u_x$ scales with the inverse of B, where $+x$ points toward the shock, antiparallel to the shock normal vector. We use the relation $u_{\rm up}B_{\rm up} = u_{\rm dn}B_{\rm dn}$ (where "up" is upstream and "dn" is downstream) in our assumption of the evolution of the flow speed, assuming the mean magnetic flux across the shock is conserved. Or, written another way, $\boldsymbol{u}(\boldsymbol{x}) = \boldsymbol{u}_{\rm up}\boldsymbol{B}_{\rm up}/\boldsymbol{B}(\boldsymbol{x})$.

Figures 2–5 show the distribution functions and modeled instrument count rates derived from our test particle simulations for each case in Figure 1. Figure 2 shows the first case where the shock compression ratio $r = 2.0$ and the upstream bulk flow speed $\boldsymbol{u}_{\rm up,sh} = 300$ km s^{-1}. In the left panel, we show the upstream (dashed curves) and downstream (solid curves) speed distributions for both SWIs and PUIs (all protons) in the plasma frame. As can be seen in the left panel, the SWIs are mainly adiabatically heated in the compressed flow, and some of the PUIs are preferentially accelerated, creating a steep tail

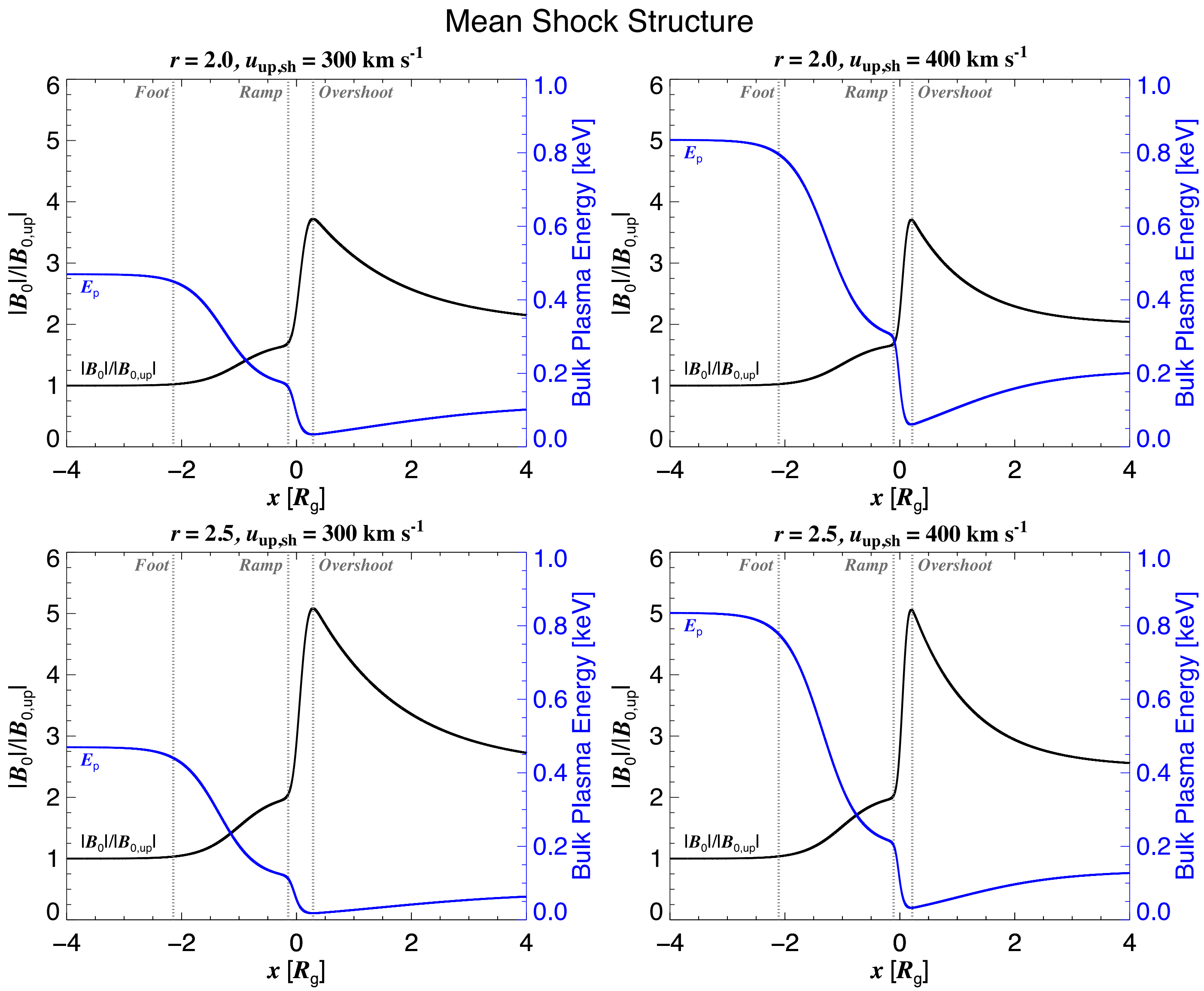

Figure 1. Mean shock profiles for four cases of the compression ratio (r = 2, 2.5) and upstream SW speed ($u_{\mathrm{up,sh}}$ = 300 km s^{-1}, 400 km s^{-1}).

slope immediately above ∼0.5 keV and a second tail slope above ∼2 keV. This second tail population consists of particles that underwent multiple reflections at the shock via shock drift acceleration (J. Giacalone & R. Decker 2010; J. Giacalone et al. 2021; E. J. Zirnstein et al. 2021), where each reflection allows the PUI to gain more energy as it gyrates in the upstream SW flow before coming back to the HTS. The first PUI population consists of particles that did not undergo such reflections due to their position in velocity space (see Figure 1 in G. P. Zank et al. 2010), so most undergo a single or no reflection before crossing downstream. In the right panel, we show the downstream count rate distributions in the spacecraft reference frame. First, we note that the dashed gray line is the average background rate that SWAP has observed in the outer heliosphere. The dashed black line is the maximum energy/charge that SWAP can measure. Finally, the solid black curve is the total of SWIs + PUIs + background rates, which is what SWAP would measure.

The downstream count rates are very different from what SWAP observes in the supersonic SW (D. J. McComas et al. 2017, 2025; E. J. Zirnstein et al. 2018; B. L. Shrestha et al. 2024). There is a crudely Maxwellian shape to the SWIs, and their count rate is low due to their higher temperature downstream of the HTS (we note, however, that the modeled downstream SWI temperature is approximately 2 times higher than that observed by Voyager 2). Second, there is no clear cutoff of the PUI distribution, but rather a hump at ∼0.8 keV, and two populations of PUIs. In this case, SWAP will be able to measure the first population and part of the second population (>2 keV q^{-1}). However, the statistics may not be good enough to discern the presence of the second population from SWAP observations if the count rates are too close to the uncertainty range of the background rate. We checked the isotropy of the downstream distribution and found that in large part the distribution is isotropic (both SWIs and PUIs), particularly in the v_x and v_z directions. There is a noticeable asymmetry in the v_y component. However, the asymmetry does not affect the results significantly. See Figures 6 and 7 for more details.

Asymmetries in the motion of particles along a certain direction can affect the results by moving the fluxes to higher or lower energies, making a speed distribution (which assumes

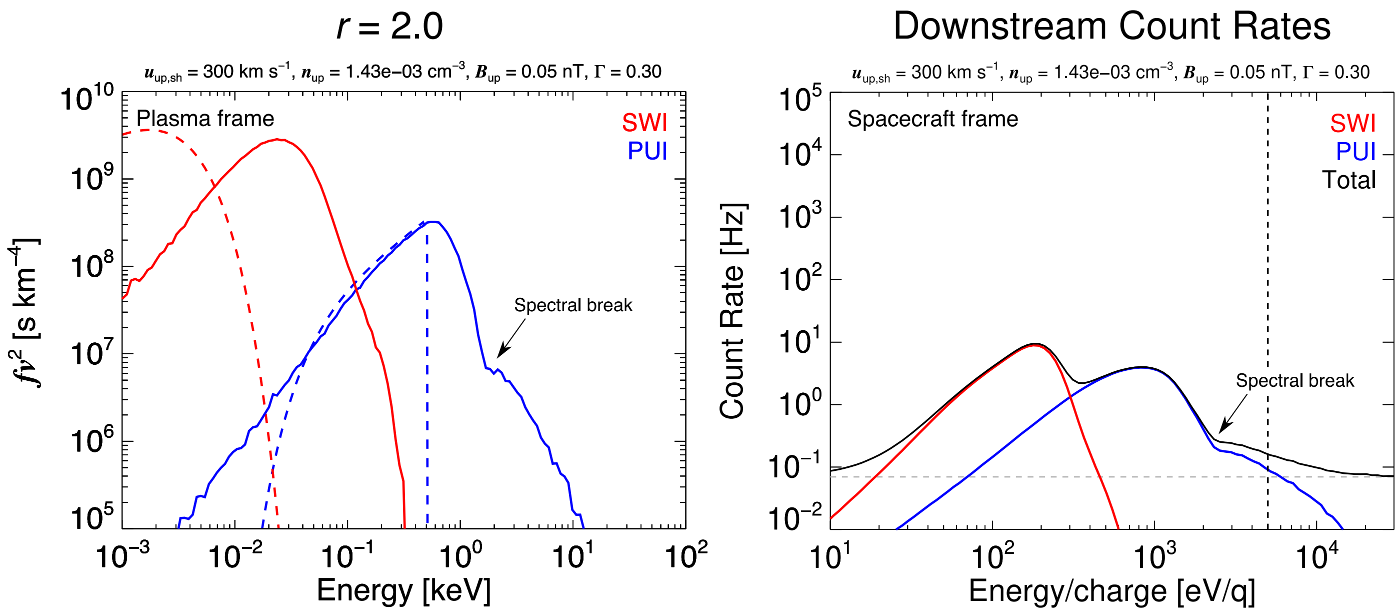

Figure 2. (Left panel) Upstream (dashed curves) and downstream (solid curves) speed distributions of the SW protons (red) and PUIs (blue) for $r = 2.0$ and $u_{\mathrm{up,sh}} = 300\ \mathrm{km\ s^{-1}}$. (Right panel) Downstream count rates in the spacecraft reference frame. The background count rate, most likely a consequence of Galactic cosmic rays (GCRs) entering the instrument, is shown as the horizontal dashed gray line. SWAP's upper energy/charge measurement limit is shown as the vertical dashed black line. Note that the distributions are nearly isotropic downstream.

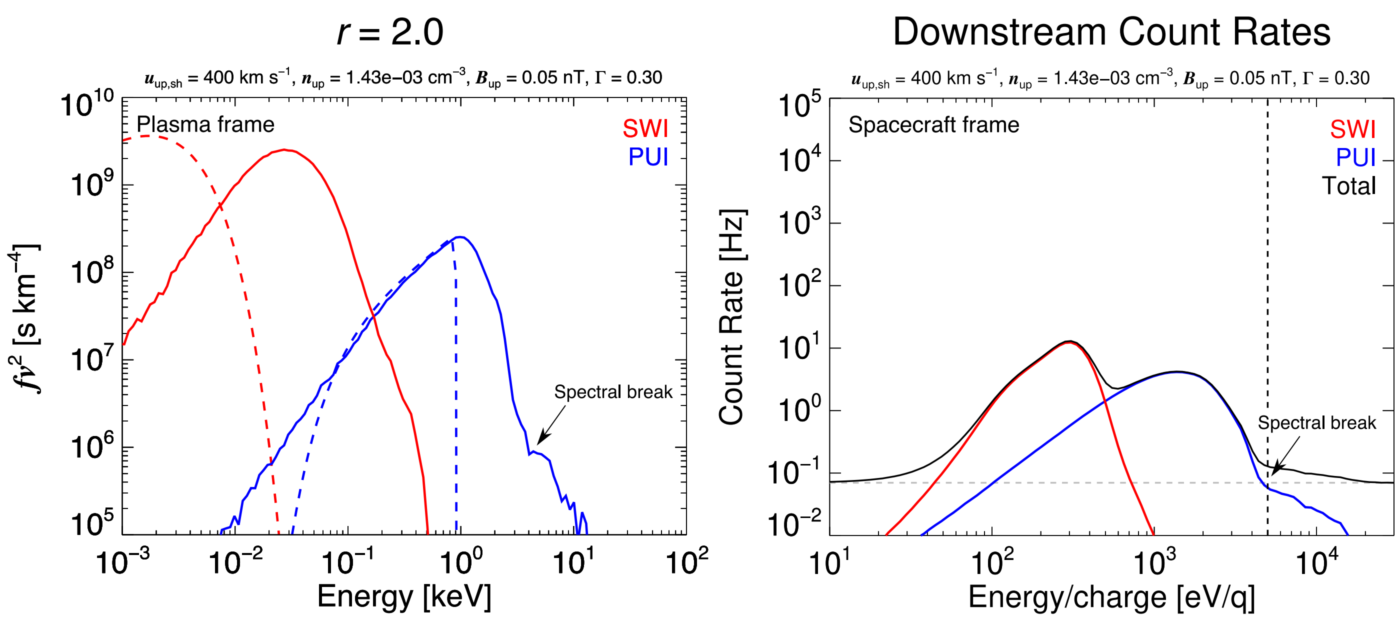

Figure 3. Same as Figure 2, except $u_{\mathrm{up,sh}} = 400\ \mathrm{km\ s^{-1}}$.

isotropy) less meaningful. The same occurs for the count rates in the spacecraft frame. If, for example, there is a high anisotropy toward the $+x$-direction (the direction of flow in our model) for PUIs, then this will appear as higher count rates at higher energies. Our results, however, show no significant anisotropies in the x-direction.

Figure 3 shows a similar case as in Figure 2, except $u_{\mathrm{up,sh}} = 400\ \mathrm{km\ s^{-1}}$. In this scenario, the faster SW speed shifts the distributions higher in energy. The break in the power law of the PUI speed distribution in the downstream plasma frame, which is clearly seen in the left panel of Figure 2, is at slightly lower intensities and occurs around ~5 keV in Figure 3. Thus, like Figure 2, the PUIs here are either merely heated across the shock or undergo multiple reflections from the shock to produce a high-energy tail. The SWI distribution is hotter due to the higher Mach number flow, and both populations are shifted to slightly higher energies because of this. In the downstream count rates in the spacecraft frame, the distributions are also shifted to higher energies, where the peak of the PUI distribution is now above 1 keV. As can be seen, the spectral break in the PUI distribution is observed near ~5 keV, which is the upper limit of SWAP's measurement capabilities. Thus, in a faster SW speed scenario with $r = 2$, SWAP probably would not be able to observe the second PUI population. Like the results shown in Figure 2, the downstream distribution is nearly isotropic. Again, there is a slight asymmetry in the v_y component, which is a bit larger than for Figure 2. This is the reason for the slight second hump in the

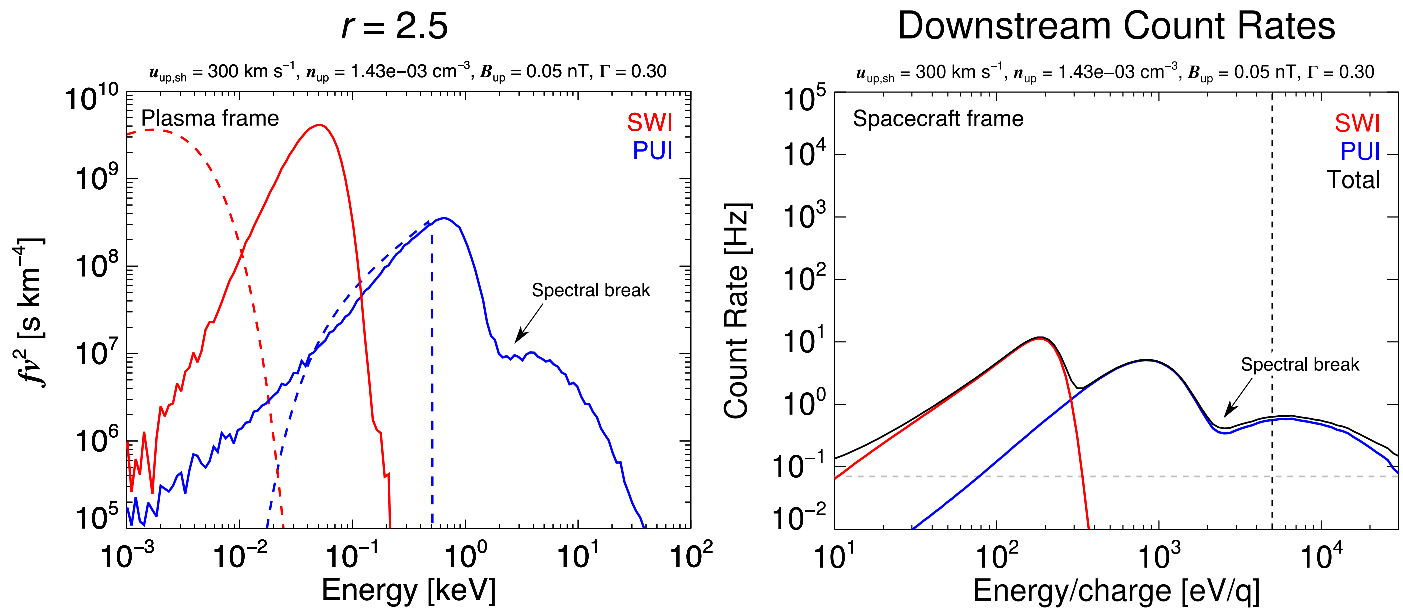

Figure 4. Same as Figure 2, except $r = 2.5$.

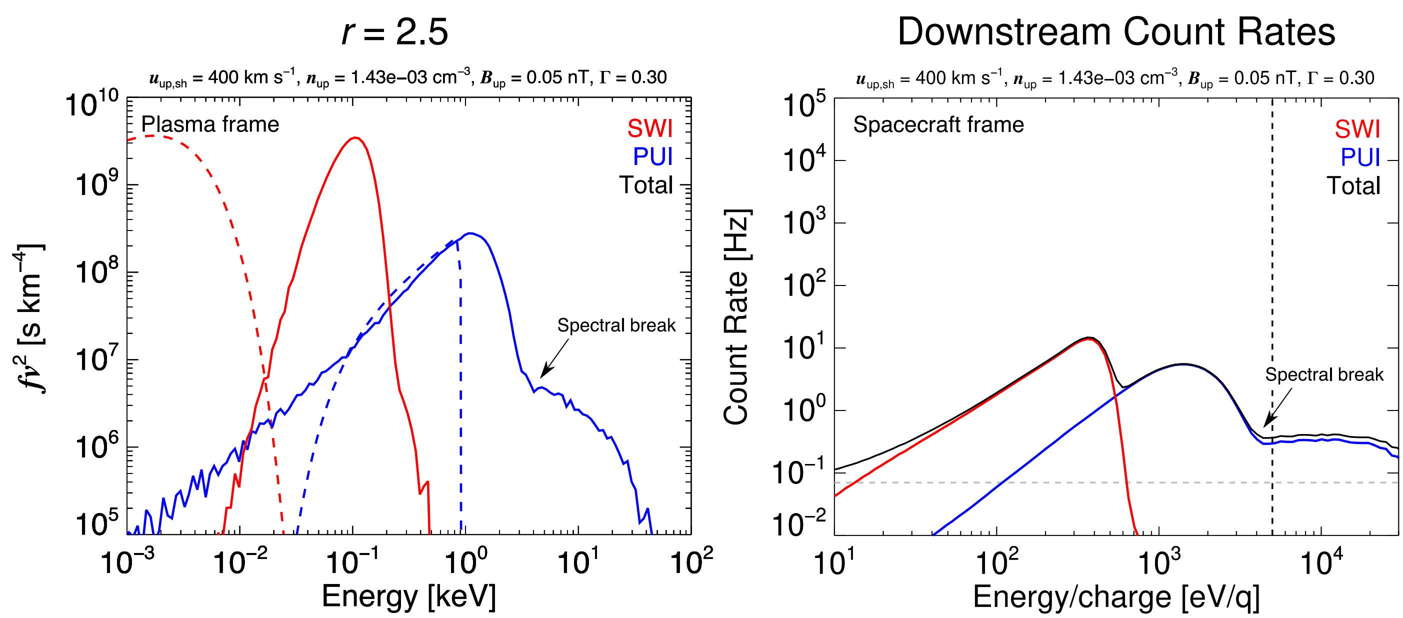

Figure 5. Same as Figure 2, except $r = 2.5$ and $u_{\mathrm{up,sh}} = 400$ km s^{-1}.

SWI count rate distribution in Figure 3, around ∼100–200 eV. The PUIs also show a visible anisotropy in the v_y component. See Figure 6 and the related discussion.

Figure 4 shows a larger compression ratio with the same upstream SW speed as Figure 2. As seen here in the downstream plasma frame, the higher compression ratio generates a larger accelerated PUI population (see left panel of Figure 4, solid blue curve), whose peak begins at ∼4 keV followed by a PUI tail and rollover at higher energies. This is because it is more difficult for some particles in velocity space to cross the shock (G. P. Zank et al. 2010), allowing for more time for reflection and acceleration of PUIs. Compared to Figure 2, the SWI distribution has gotten narrower and less Maxwellian-like in the plasma frame, and the peak of the distribution has shifted to higher energies due to the higher compression ratio (i.e., more energy required to cross the shock). In the spacecraft frame, the count rates show a significant secondary PUI bump, whose peak is at an energy of ∼7 keV and thus above the limit of SWAP's energy range. However, SWAP may be able to measure the dip and rise in between the first and second PUI populations, allowing us to better understand the potential presence of a second population, likely formed from PUIs preferentially accelerated at the HTS. We can imagine that if the SW is even slower than ∼300 km s^{-1}, it is more likely that SWAP could see the second, accelerated PUI population. See Figure 6 for information related to anisotropies of the distribution.

Finally, Figure 5 shows the case where both r and $u_{\mathrm{up,sh}}$ are higher. Similar to Figure 3, increasing the SW speed would make it difficult for SWAP to observe the second population in the downstream count rate distribution. The second PUI population begins almost at the same energy as SWAP's

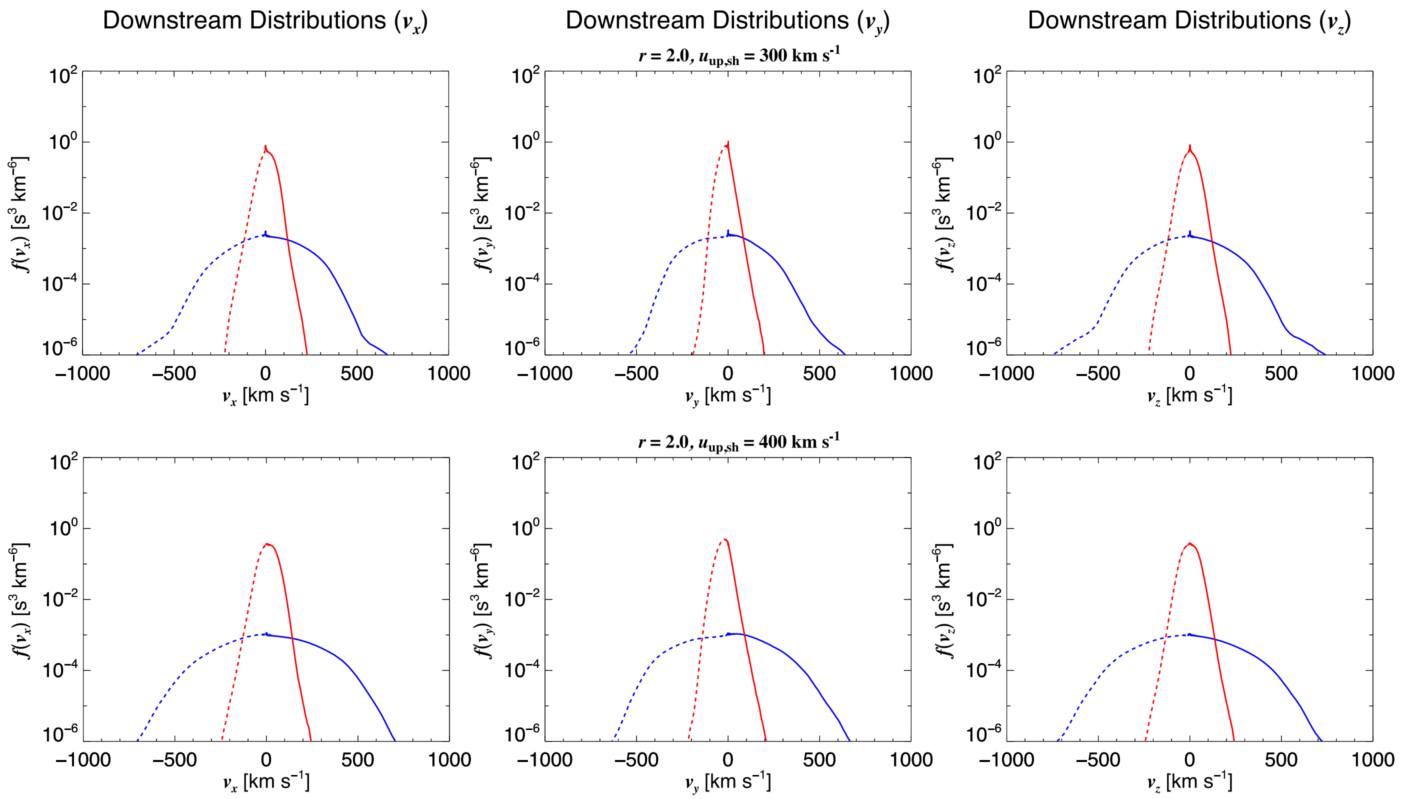

Figure 6. Components of the downstream speed distributions for results shown in Figures 2 and 3.

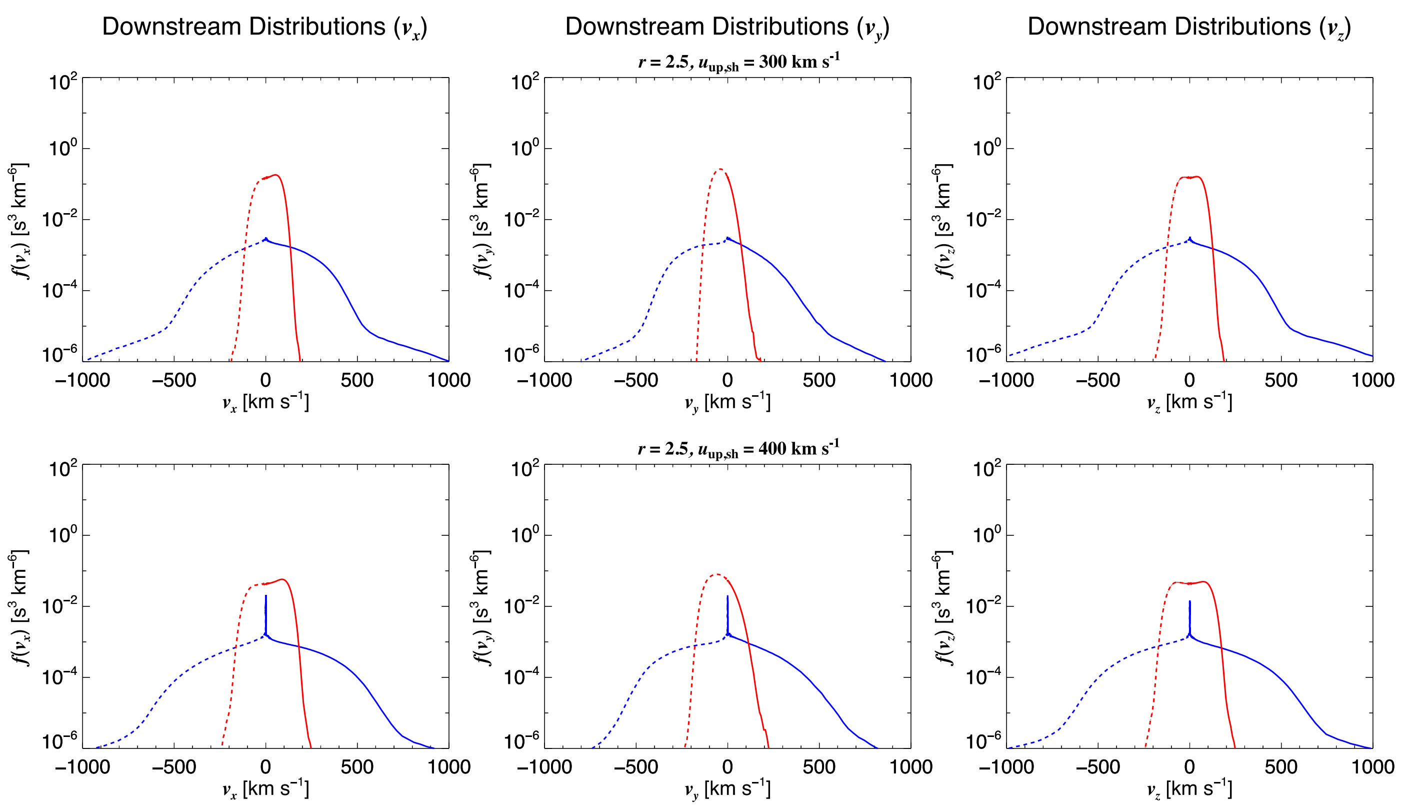

Figure 7. Components of the downstream speed distributions for results shown in Figures 4 and 5.

energy cutoff (∼5 keV in the spacecraft frame) and has a rollover above ∼20 keV in the plasma frame and above ∼30 keV in the spacecraft frame. Like in Figure 3, the faster SW speed shifts the distributions to higher energies, and like in Figure 4, the higher compression ratio yields a larger accelerated PUI population. Note, however, the difference between Figures 3 and 5. Figure 5 has the same upstream SW speed, but a larger compression ratio. First, if SWAP was able to take measurements at higher energies, it may see a flat distribution between ∼5 up to ∼30 keV. Second, though SWAP does not measure above 5 keV, it would be able to see the first, primary bump in the PUI count rate distribution, and the count rates do not decrease to the background noise floor before the secondary PUI population takes over, unlike what happens with a smaller compression ratio (right panel of Figure 3). This subtle difference, along with all our results shown in Figures 2–5, are important to consider when deriving the moments of the SWAP observations beyond the HTS. See Figures 6 and 7 for information related to anisotropies of the distribution.

We show the v_x, v_y, and v_z components of the downstream velocity distributions in Figures 6 and 7 for each case presented in Figures 2–5. In general, the SWI and PUI distributions (blue) show little anisotropy in the v_x (and v_z) components, though there is some asymmetry in the v_y component, especially when the compression ratio is 2.5 (see differences between the solid and dashed curves in Figure 6, middle column). We note that the mean field is along the $+y$-direction, so it is possible there is a particle drift along the mean field. However, we are mainly concerned with the PUI component of the distribution in this study. The results of the PUI component are approximately isotropic downstream of the shock, especially considering that the v_z component is similar to the v_x component. Therefore, we believe that our results are reliable at least qualitatively, and it is reasonable to say the PUI results are quantitatively reliable. This is partly because SWAP cannot determine the directionality of its measured counts and thus analyses of SWAP observations assume the PUI distribution is isotropic in the plasma frame (D. J. McComas et al. 2017). Our modeled distributions are nearly isotropic, at least for the PUIs (see Figure 6).

4. Discussion and Conclusions

In this study we have demonstrated what the New Horizons SWAP instrument may observe once it crosses the HTS. We used a test particle simulation (E. J. Zirnstein et al. 2021) to propagate SWIs and PUIs (all protons) across the HTS in the presence of isotropic turbulence (see Appendix). The test particle simulation shows, for most cases, that there is a break in the PUI distribution that leads to a higher energy, secondary population of PUIs that were preferentially accelerated at the HTS via shock drift acceleration (J. Giacalone & R. Decker 2010; J. Giacalone et al. 2021; E. J. Zirnstein et al. 2021), e.g., see Figures 4(a) and 5(b) in E. J. Zirnstein et al. (2021).

As can be seen in Figures 2–5, the downstream count rate distributions will be very different from what SWAP observes in the supersonic SW. This implies a new method of fitting to the count rate distributions will be required to derive moments of the downstream SWIs and PUIs, because (1) the SWIs are much hotter in the heliosheath and thus produce a lower peak count rate, making it slightly more difficult finding the bulk SW speed, (2) SW alpha particles can complicate finding the SW proton properties (alphas are not modeled here), and (3) the PUIs can no longer be represented by a filled shell distribution, as has been done in the past (D. J. McComas et al. 2017, 2021, 2022, 2025). Also, there is a clear secondary population of PUIs, which SWAP will have difficulty measuring due to the maximum limit of its energy range, which was lowered in 2021 August because the engineering data indicated that SWAP may be reaching the edge of its high-voltage performance (D. J. McComas et al. 2022). Near the maximum energy (∼5 keV), the count rates of the secondary PUI population have nearly reached the background noise floor (dashed gray line) for the low compression ratio and slower SW speed case shown in Figure 2. We do not know what the background noise floor will be once SWAP is in the heliosheath, but if it originates from galactic cosmic rays (GCRs), we expect the noise floor to increase (V. Florinski et al. 2003). While the filtering of GCRs trying to enter the heliosphere in the heliosheath has been shown to vary with distance by Voyager measurements (Figure 34 in J. S. Rankin et al. 2022), our results are only applicable to just downstream of the shock, and not through the heliosheath. Therefore, the GCR modulation by the heliosheath is unlikely to be seen at the shock crossing.

By increasing the upstream SW speed from 300 to 400 km s^{-1}, the count rate distribution shifted to higher energies, thus making it more unlikely for SWAP to detect the secondary PUI population (Figure 3). Increasing the HTS compression ratio from 2 (like that observed by Voyager 2; J. D. Richardson et al. 2008) to 2.5, the secondary PUI population becomes more intense and produces higher count rates at energies >2–3 keV. SWAP may be able to observe part of the secondary population, if the upstream SW speed is not too high. We note that the results of our simulations, particularly for the PUIs, are similar to those derived from a hybrid simulation with a more realistic simulation of the HTS surface (J. Giacalone et al. 2021). Therefore, we believe our model predictions are a fairly accurate representation of what to expect.

In this study we assumed that the HTS in the direction of New Horizons' trajectory is 90 au from the Sun. If the HTS was closer, we would expect SWAP to observe a similar downstream count rate distribution as shown in Figures 2–5, depending on the compression ratio and upstream SW speed. We have tested this assumption by simulating a shock at 70 au from the Sun, and besides differences in density of the downstream distributions, the results are very similar (see the Appendix). We posit that an energetic particle precursor, like the one observed at Voyager 2's crossing of the HTS (R. B. Decker et al. 2008; V. Florinski et al. 2009), will likely be present upstream of the HTS, and SWAP may observe a slowing of the SW ahead of the HTS crossing. With SWAP near the ecliptic plane, it will likely observe SW speeds ahead of the HTS between 300 and 400 km s^{-1}, after having been slowed down by an energetic particle precursor. Thus, as New Horizons gets closer to the HTS, we anticipate modeling to improve our predictions of the downstream distribution (e.g., the hybrid simulation results from J. Giacalone et al. (2021) may be converted to count rates in the spacecraft frame), and the SWAP instrument team to have a better understanding of how to extract distribution moments from the measurements downstream of the HTS.

Finally, one of the most interesting aspects of New Horizons' crossing of the HTS is the ability to use the Heliophysics System Observatory to connect the first, in situ observations of PUIs in the outer heliosphere simultaneously with the heliosheath ENA maps that will be measured by the Interstellar Mapping and Acceleration Probe (IMAP; D. J. McComas et al. 2018). IMAP is equipped with three ENA imagers whose combined energy range surpasses ∼100 keV. The PUI distribution observed by SWAP may be able to be connected to the intensity and slope of the heliosheath-originating ENA spectrum measured at Sun–Earth Lagrange point 1, where IMAP will be taking measurements from, and help us learn more about particle heating in the heliosheath.

Acknowledgments

We thank everyone who made the New Horizons mission possible. This work was supported by the New Horizons mission (M99023MJM; PU-AWD1006357) as part of NASA's New Frontiers program. This work was also partially supported by NASA's IMAP mission (80GSFC19C0027). E. J.Z. and B.S. acknowledge partial support from NASA's Heliophysics Supporting Research grant 80NSSC21K1686. The work in this study was performed at the TIGRESS high-performance computer center at Princeton University, which is jointly supported by the Princeton Institute for Computational Science and Engineering and the Princeton University Office of Information Technology's Research Computing department.

Appendix

To simulate turbulence in our test particle model, we sum over many synthetic wave modes over a large wavenumber range. The total field is given as $\boldsymbol{B} = \boldsymbol{B}_{\rm m} + \delta\boldsymbol{B}$, where $\delta\boldsymbol{B}$ is the turbulent component (J. Giacalone & J. R. Jokipii 1999) and $\boldsymbol{B}_{\rm m}$ is the mean field structure of the shock (Figure 1). The turbulent component can be written in Cartesian coordinates as

$$\delta\boldsymbol{B}(x, y, z) = \sum_{n=1}^{N} A(k_n)\hat{\boldsymbol{\xi}}_n \exp(ik_n z'_n + i\beta_n), \tag{A1}$$

$$\hat{\boldsymbol{\xi}}_n = \cos\alpha_n \boldsymbol{x}'_n + i\sin\alpha_n \boldsymbol{y}'_n, \tag{A2}$$

$$\begin{pmatrix} x' \\ y' \\ z' \end{pmatrix} = \begin{pmatrix} \cos\theta_n\cos\varphi_n & \cos\theta_n\sin\varphi_n & -\sin\theta_n \\ -\sin\varphi_n & \cos\varphi_n & 0 \\ \sin\theta_n\cos\varphi_n & \sin\theta_n\sin\varphi_n & \cos\theta_n \end{pmatrix}\begin{pmatrix} x \\ y \\ z \end{pmatrix}, \tag{A3}$$

$$A^2(k_n) = 2\sigma^2 G(k_n) \Big/ \left[\sum_{n=1}^{N} G(k_n)\right], \tag{A4}$$

$$G(k_n) = \frac{C_n}{1 + (k_n L_c)^{\gamma}}, \tag{A5}$$

where $N = 400$ is the number of wave modes (about ∼80 wave modes per decade), with wavevector direction angles θ_n and φ_n, correlation length $L_{\rm c}$, wave variance σ^2, wavenumber $k_{\rm n}$, polarization α_n, phase β_n, and spectral index γ. The turbulence wave variance is chosen to be $\sigma^2 = (0.05\ {\rm nT})^2$, following E. J. Zirnstein et al. (2021) and consistent with Voyager 2 observations. The correlation length is set to $L_{\rm c} = 0.17$ au (J. Giacalone & R. Decker 2010; E. J. Zirnstein et al. 2021). The minimum and maximum wavenumbers are set to $0.01/R_{g,w}$ and $1000/R_{g,w}$, where $R_{g,w}$ is the gyroradius of a 640 km s^{-1} proton in the upstream magnetic field (note that we choose 640 km s^{-1} so that we can cover a large enough wavelength for accelerated particles in our domain).

The mean field is assumed to be perpendicular to the shock normal vector (i.e., a perpendicular shock) for simplicity in our analysis. Also, we simulate isotropic turbulence in this study, such that the wavevectors' directions, polarizations, and phases are distributed randomly in space. In other words, we randomly select from a uniform distribution the variables in the following ranges: $-1 < \cos(\theta_n) < 1$, $0 < \varphi_n < 2\pi$, $0 < \alpha_n < 2\pi$, and $0 < \beta_n < 2\pi$. Finally, the variable $C_n = 4\pi k_n^2 \Delta k_n$ and $\gamma = 11/3$ for isotropic turbulence (J. Giacalone & J. R. Jokipii 1999). It is not known how isotropic the turbulence is downstream of the HTS, even from Voyager 2 observations (L. F. Burlaga et al. 2008). Therefore, the choice of using isotropic turbulence here is made mostly for convenience. In theory, E. J. Zirnstein et al. (2021) have shown there is little change to the PUI component of the distribution when compared to composite turbulence (slab + 2D) downstream of the shock, as shown in their Figure 3.

The cross-shock potential in the electric field term shown in Equation (1) is approximated by (E. J. Zirnstein et al. 2021)

$$e\Phi(x) \cong \Lambda\left(\frac{\gamma}{\gamma - 1}k_{\rm B}T_e(x) + \frac{B_u}{\mu_0 n_u}(B_y(x) - B_{0,u,y})\right), \tag{A6}$$

as a function of position along the shock normal. Equation (A6) includes the effects of electron energy (first term) and magnetic field energy (second term). The parameter $\Lambda = 2.71$ is a scaling factor that accounts for the extra energy from flow deflection at the shock (the chosen value is explained in the Appendix of E. J. Zirnstein et al. 2021), and yields a peak potential energy at the shock consistent with particle-in-cell simulations (R. Kumar et al. 2018). Equation (A6) here is written similarly to M. M. Leroy (1983; see their Equation (15)), though we estimate the flow deflection term, which is folded into Λ, and like G. P. Zank et al. (1996; see their Equation (A6)), though they use a simpler form.

We tested the effects of an HTS at a closer distance from the Sun compared to the main results of the Letter. We do this by simulating a shock at 70 au from the Sun, with physical quantities consistent with this distance, such as SWI density (0.002 cm^{-3}), PUI density ratio (0.22), magnetic field strength (0.065 nT), and PUI cooling index (2.5). The compression ratio and upstream SW speed are the same as in Figure 3. The results for an HTS at 70 au are shown in Figure 8. Besides the fluxes and count rates being slightly higher due to the larger density at 70 au (higher by a factor of ∼2 as compared to Figure 3), there is no significant difference between our results at 70 versus 90 au.

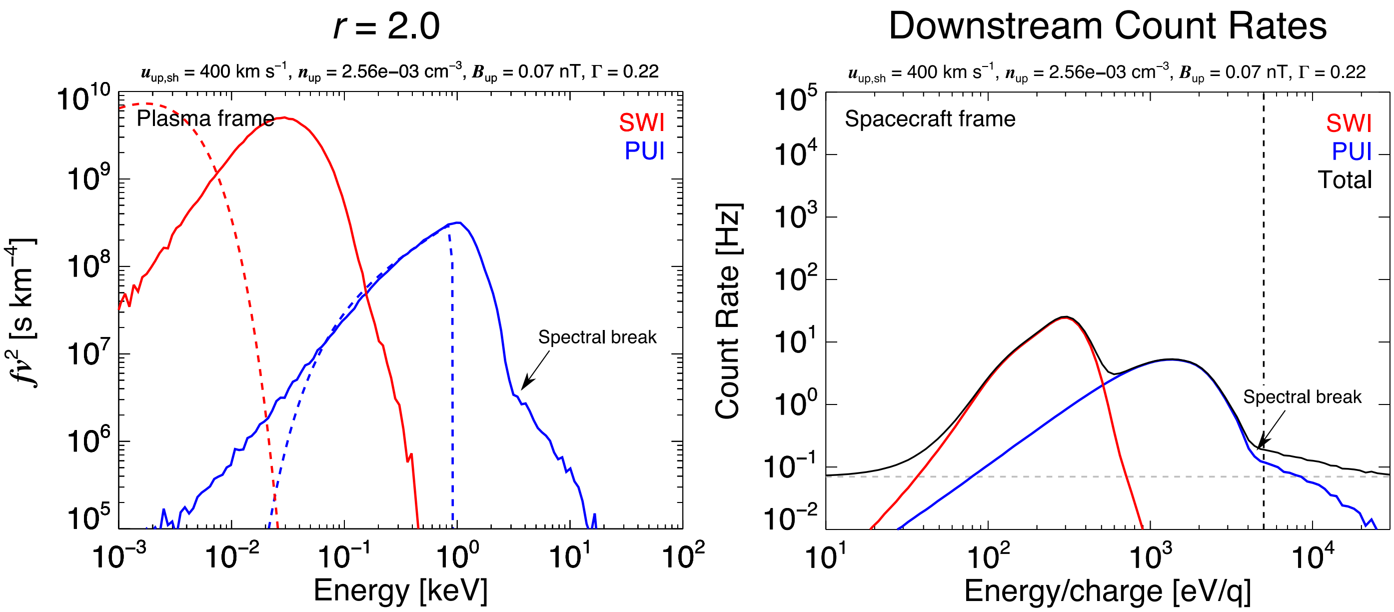

Figure 8. Similar to Figure 3, except the HTS location is at 70 au from the Sun. See text for details on the upstream SW parameters.

ORCID iDs

E. J. Zirnstein https://orcid.org/0000-0001-7240-0618
D. J. McComas https://orcid.org/0000-0001-6160-1158
B. L. Shrestha https://orcid.org/0000-0002-5247-4107
H. A. Elliott https://orcid.org/0000-0003-2297-3922
P. C. Brandt https://orcid.org/0000-0002-4644-0306
S. A. Stern https://orcid.org/0000-0001-5018-7537
A. R. Poppe https://orcid.org/0000-0001-8137-8176
J. Parker https://orcid.org/0000-0002-3672-0603
E. Provornikova https://orcid.org/0000-0001-8875-7478
K. Singer https://orcid.org/0000-0003-3045-8445
A. Verbiscer https://orcid.org/0000-0002-3323-9304

References

Ariad, D., & Gedalin, M. 2013, JGRA, 118, 2854
Burlaga, L. F., Ness, N. F., Acuña, M. H., et al. 2008, Natur, 454, 75
Burrows, R. H., Zank, G. P., Webb, G. M., Burlaga, L. F., & Ness, N. F. 2010, ApJ, 715, 1109
Decker, R. B., Krimigis, S. M., Roelof, E. C., et al. 2008, Natur, 454, 67
Elliott, H. A., McComas, D. J., Valek, P., et al. 2016, ApJS, 223, 19
Fahr, H. J. 1971, A&A, 14, 263
Florinski, V., Decker, R. B., le Roux, J. A., & Zank, G. P. 2009, GeoRL, 36, L12101
Florinski, V., Zank, G. P., & Pogorelov, N. V. 2003, JGRA, 108, 1228
Giacalone, J., & Decker, R. 2010, ApJ, 710, 91
Giacalone, J., & Jokipii, J. R. 1999, ApJ, 520, 204
Giacalone, J., Nakanotani, M., Zank, G. P., et al. 2021, ApJ, 911, 27
Kumar, R., Zirnstein, E. J., & Spitkovsky, A. 2018, ApJ, 860, 156
Leroy, M. M. 1983, PhFl, 26, 2742
Livadiotis, G., McComas, D. J., & Shrestha, B. L. 2024, ApJ, 968, 66
Matsukiyo, S., & Scholer, M. 2014, JGRA, 119, 2388
McComas, D., Allegrini, F., Bagenal, F., et al. 2008, SSRv, 140, 261
McComas, D. J., Christian, E. R., Schwadron, N. A., et al. 2018, SSRv, 214, 116
McComas, D. J., Shrestha, B. L., Livadiotis, G., et al. 2025, ApJ, 980, 154
McComas, D. J., Shrestha, B. L., Swaczyna, P., et al. 2022, ApJ, 934, 147
McComas, D. J., Swaczyna, P., Szalay, J. R., et al. 2021, ApJS, 254, 19
McComas, D. J., Zirnstein, E. J., Bzowski, M., et al. 2017, ApJS, 233, 8
Press, W. H., Teukolsky, S. A., Vetterling, W. T., & Flannery, B. P. 2002, Numerical Recipes in C: The Art of Scientific Computing (2nd ed.; Cambridge: Cambridge Univ. Press)
Randol, B. M., Elliott, H. A., Gosling, J. T., McComas, D. J., & Schwadron, N. A. 2012, ApJ, 755, 75
Rankin, J. S., Bindi, V., Bykov, A. M., et al. 2022, SSRv, 218, 42
Richardson, J. D., Kasper, J. C., Wang, C., Belcher, J. W., & Lazarus, A. J. 2008, Natur, 454, 63
Shrestha, B. L., McComas, D. J., Zirnstein, E. J., et al. 2025, ApJ, 984, 11
Shrestha, B. L., Zirnstein, E. J., McComas, D. J., et al. 2024, ApJ, 960, 35
Swaczyna, P., McComas, D. J., Zirnstein, E. J., et al. 2020, ApJ, 903, 48
Thomas, G. E. 1978, AREPS, 6, 173
Wang, B., Zank, G. P., Shrestha, B. L., Kornbleuth, M., & Opher, M. 2023, ApJ, 944, 198
Yang, Z., Liu, Y. D., Richardson, J. D., et al. 2015, ApJ, 809, 28
Zank, G. P., Adhikari, L., Zhao, L.-L., et al. 2018, ApJ, 869, 23
Zank, G. P., Heerikhuisen, J., Pogorelov, N. V., Burrows, R., & McComas, D. 2010, ApJ, 708, 1092
Zank, G. P., Pauls, H. L., Cairns, I. H., & Webb, G. M. 1996, JGRA, 101, 457
Zirnstein, E. J., Kumar, R., Bandyopadhyay, R., et al. 2021, ApJL, 916, L21
Zirnstein, E. J., McComas, D. J., Kumar, R., et al. 2018, PhRvL, 121, 075102
Zirnstein, E. J., Möbius, E., Zhang, M., et al. 2022, SSRv, 218, 28